THE AMERICAN SOCIETY OF MECHANICAL ENGINEERS
345 E. 47th St., New York, N.Y. 10017

96-GT-207

EFFECT OF PERIODIC WAKE PASSING ON FILM EFFECTIVENESS OF INCLINED DISCRETE COOLING HOLES AROUND THE LEADING EDGE OF A BLUNT BODY

Ken-ichi Funazaki, Eitaro Koyabu
Department of Mechanical Engineering, Iwate University, Morioka, Japan

and

Shigemichi Yamawaki
Aero-Engine and Space Operation, Ishikawajima-Harima Heavy Industries Co., Tokyo, Japan

ABSTRACT

Detailed studies are conducted on film effectiveness of inclined discrete cooling holes around the leading edge of a blunt body that is subjected to periodically incoming wakes as well as free-stream turbulence with various levels of intensity. The cooling holes have a configuration similar to that of a typical turbine blade and are angled at 30 and 90 degree to the surface in the spanwise and streamwise directions, respectively. A spoked-wheel type wake generator is used in this study to simulate periodically incoming wakes to turbine blades. In addition, two types of turbulence grids are used to elevate a free-stream turbulence intensity. We adopt three blowing ratios of the secondary air to the mainstream. Most of the dominant flow conditions are reproduced in this study except for the air density ratio of the secondary air and the main stream. For each of the blowing ratios, wall temperature around the surface of the test model are measured by thermocouples situated inside the model. The temperature is visualized using liquid crystals to obtain traces of the injected secondary air on the test surface, which consequently helps us interpret the data of the thermocouples.

NOMENCLATURE

B	:Mean blowing ratio $=\rho_2 U_2 / \rho_\infty U_\infty$
B_{15}, B_{40}	:Local blowing ratio
D	:Leading edge diameter
d	:Cooling hole diameter
d_g	:Diameter of the turbulence grid wire
f	:Wake passing frequency ($=nn_c / 60$)
h	:Heat transfer coefficient
L	:Axial gap between the turbulence grid and the model leading edge
l	:Axial gap between the wake generator and the model leading edge
L_e	:Streamwise dissipation length of free-stream turbulence and wake turbulence
M	:Grid mesh size of the turbulence grid
Nu_D	:Nusselt number based on the leading edge diameter
n, n_c	:Rotating speed and the number of wake generating bars
R	:Radius of the leading edge
Re_D	:Reynolds number based on the diameter of the leading edge and the inlet velocity$= U_\infty D / \nu$
S	:Strouhal number$= fD / U_\infty$
T, T_{aw}	:Temperature, adiabatic wall temperature
$Tu(t)$	:Turbulence intensity
Tu_b	:Back ground turbulence intensity
U_{local}	:Local flow velocity around the model surface
U_∞	:Inlet velocity
u'	:Streamwise velocity fluctuation
V_{out}	:Outlet velocity
v	:Velocity on the model surface
x	:Axial distance measured from the leading edge
x_{surf}	:Distance along the surface from the stagnation on the leading edge
η	:Film effectiveness $=(T_{aw}-T_\infty)/(T_2-T_\infty)$

Subscripts

∞,2	:mainstream, secondary air
15,40	:first row, second row

INTRODUCTION

To improve the performance of gas turbines, specifications for turbine inlet temperature have been increasing over the past several decades. Film cooling is an effective method for protecting blade surfaces from high temperature combustion gas and there have been many investigations on the thermo-fluid characteristics of film cooling. The leading edge film cooling of turbine blades, which is our concern in this study, has been also attracting attentions from many researchers (Mick and Mayle (1988), Mehendale et al. (1992), Salcudean et al. (1994)).

As Funazaki et al. (1995#1) pointed out, the heat load observed at the leading edge of turbine blades is greatly affected by free-stream turbulence as well as periodic wake passage, hence one can easily imagine that these flow disturbances have some influences on film cooling at the leading edge. Funazaki et al. (1995#2) accordingly studied

Presented at the International Gas Turbine and Aeroengine Congress & Exhibition
Birmingham, UK — June 10-13, 1996
This paper has been accepted for publication in the Transactions of the ASME
Discussion of it will be accepted at ASME Headquarters until September 30, 1996

the influence of periodic wake passing as well as free-stream turbulence on the film effectiveness of discrete cooling holes over the leading edge of a blunt body. Their test model had a realistic geometrical configuration of cooling holes except for the injection angle. Their injection angle was normal to the surface. They found that the film effectiveness at lower blowing ratio greatly deteriorated due to the wake passing and the free-stream turbulence. Although their findings are useful for understanding how the film effectiveness of the leading edge cooling holes behaves under the realistic flow environment, they are not applicable to modern turbine cooling design in a straightforward manner because of the injection angle adopted in their study.

This study therefore focuses on the effect of periodic passing wakes on film effectiveness of spanwisely-inclined cooling holes on the leading edge under several free-stream turbulence conditions. The model used in this study has the same geometry as the previous study, consisting of a semi-circular leading edge and two flat plates. Spanwise angle of each of the cooling holes is 30° measured from the model surface, which is commonly used in modern turbine blades. The upstream periodic wakes is produced by a spoked-wheel type wake generator. The free-stream turbulence is generated by turbulence grids. We adopt three blowing ratios of the secondary air to the mainstream. For each of the blowing ratios, adiabatic wall temperature around the test surface influenced by the wakes as well as the free-stream turbulence is measured by thermocouples.

The temperature distribution is visualized using a liquid crystal sheet in order to obtain traces of the injected secondary air on the test surface. These traces will be compared with the data of the surface thermocouples in order to clarify the relationship between the measured film effectiveness and the injected air.

TEST APPARATUS AND INSTRUMENTS

A schematic layout of the test apparatus is shown in Figure 1. This apparatus is the same as that used in previous study by Funazaki et al. (1995#2). Main flow rate is adjusted by the inlet valve of the blower. Air from the blower passes through the settling chamber to the contraction nozzle with the exit cross section of 240mm x 350mm. The test channel containing the test model is inserted into the transition duct which is attached to the contraction nozzle. To remove the upstream boundary layer, the front portion of the test channel has a sharp edge and some amount of air is discharged from the clearance between the test channel and the transition duct. The transition duct has a slot through which the wake generating bars of the wake generator can pass. These wake generating bars, 5 mm diameter and 250 mm length, are mounted on the disk rim. The rotational speed of the disk is controlled by transmission gear box connected to an induction motor. The rotational speed ranges from 900 through 1500 rpm. A turbulence grid is attached to the contraction nozzle exit which is 300mm upstream of the test model leading edge and 100 mm upstream of the wake generator. Two types of grids are used and details of the grid configurations are shown in Table 1. It is revealed that these "passive type" grids generate realistic turbulence intensity levels encountered in front of turbine rotor blades (Funazaki et al. (1995#2)).

The secondary air supplied from the second blower to the film holes is heated before a laminar-flowmeter. Accordingly, the film air temperature is higher than the free-stream temperature, which means we can not simulate the density ratio of the secondary air to the mainstream air in an actual engine.

The cross section of the test channel is 200 mm height and 300 mm width and its length is 1000 mm. The test model consists of a semi-circular leading edge of 100 mm diameter and two flat plates, shown in Figure 2. The test model is assembled with acrylic-resin parts of 10 mm thickness and 200 mm height. Two rows of cooling holes of d =10 mm diameter and 40 mm ($4d$) pitch are located at ±15° and ±40° from the model center line. Axes of the holes are spanwisely inclined by 30°. The ratio of the leading edge diameter and the cooling hole diameter D/d is 10. We will refer to the film holes at ±15° and ±40° as "the first row" and "the second row", respectively. The inner surface of the test model is covered with insulator except for the leading edge.

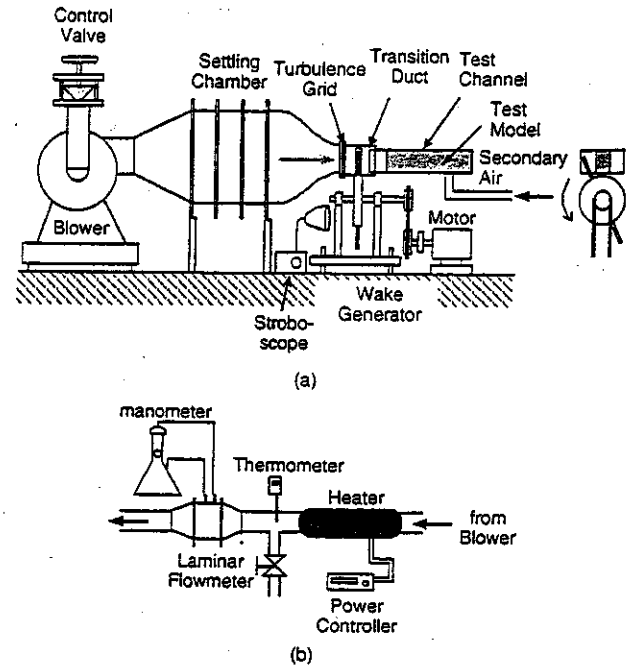

Figure 1 Test apparatus
(a) Wind tunnel (b) Secondary air supply system

Table 1 Configurations of turbulence grids and the characteristics of the turbulence generated by each grid

	Grid 1	Grid 3	No Grid
Wire Diameter (d_g)	0.8 mm	5.0 mm	-
Mesh Width (M)	5.0 mm	30.0 mm	-
Degree of Openness	0.7	0.69	-
M/d_g	6.25	6	-
Tu_b	1.50%	4.00%	0.80%
L_e	2.8 mm	7.8 mm	-

Figure 3 shows the location of the thermocouples and the film holes. The test model has 74 thermocouples embedded on the model surface to measure an adiabatic surface temperature distribution. The secondary air temperature is measured in the middle of the plenum chamber inside the model. A temperature on the inner surface of the model is also measured to check the adiabatic wall condition. Free-stream temperature is measured near the lower end of the leading edge stagnation line. All thermocouples are connected to a datalogger controlled by a personal computer. These temperature data are then averaged over 10 samples acquired within a minite to calculate time-averaged wall temperature distributions.

Pressure distributions around the test model are obtained using the test model of the same dimensions as the present one except for cooling holes, as had been employed by Funazaki (Funazaki, 1994). Local flow velocity U_{local} is then determined from those data.

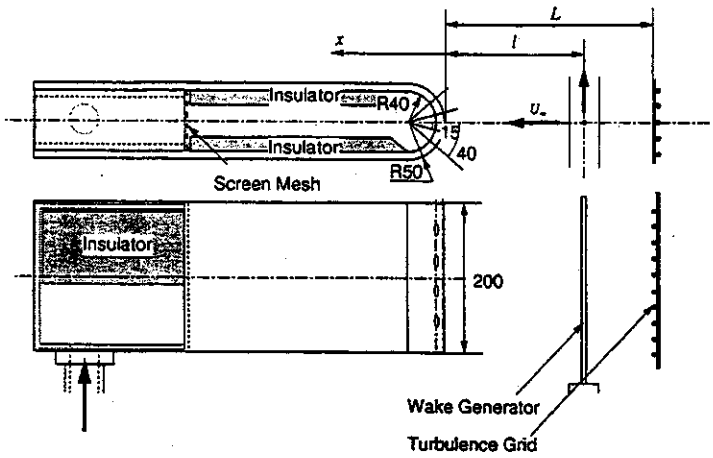

Figure 2 Test model

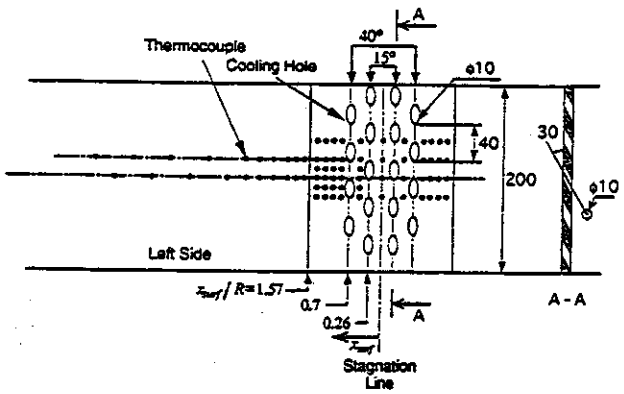

Figure 3 Layout of the film holes and locations of thermocouples on unholded surface view

The temperature distribution is visualized using a liquid crystal sheet of 0.1mm thickness (RW3040; Nippon Capsule Products). The sheet is pasted around the test model. The color changes in a temperature range of 30~40°C. Due to this broad range, it is difficult to get a sharp image of colored temperature distribution, however, the liquid crystal provides us a brief image about how the injected air spreads over the test model, which can be used for interpreting the temperature data of the surface thermocouples.

EXPERIMENT

In the present study, normalized parameters adopted in this study except for Mach number are comparable to those encountered in a real turbomachine. The inlet free-stream velocity was about 20m/s and the Reynolds number Re_D based on the leading edge diameter was 120000. The rotational speed of the wake generator was 900,1260, and 1500 rpm. The corresponding Strouhal number S, defined as

$$S = fD/U_\infty , \quad f = nn_c/60 \qquad (1)$$

was 0.24, 0.34 and 0.40.

Unsteady velocity measurements were already conducted using a hot-wire anemometer in the previous study (Funazaki et al. (1995#2)) and those data, such as ensemble-averaged velocity or time-resolved turbulence intensity were used to describe the unsteady flow field around the leading edge of the model.

The blowing ratio B, one of the most dominant parameters for film cooling, is defined as

$$B = \rho_2 U_2 / \rho_\infty U_\infty . \qquad (2)$$

All experiments were conducted at B=0.4, 0.8, or 1.2. Although this blowing ratio is a convenient parameter for this type of experiment, local blowing ratio at each row is also an important quantity for understanding the local film cooling performance. The local blowing ratio is defined as

$$B_{15} = \frac{\rho_{2,15} U_{2,15}}{\rho_{\infty,15} U_{\infty,15}} , \quad B_{40} = \frac{\rho_{2,40} U_{2,40}}{\rho_{\infty,40} U_{\infty,40}} . \qquad (3)$$

Figure 4 shows the analytical result of the relationship between the local and mean blowing ratios, indicating that these relationships differ for each row (For the detailed procedure to derive this result, refer to the appendix of Funazaki et al. (1995#2)). The local blowing ratio B_{15} varies significantly with B, in contrast to the behavior of B_{40}.

Film effectiveness η is defined as

$$\eta = (T_{2w} - T_\infty)/(T_2 - T_\infty) , \qquad (4)$$

where T_{aw} is the adiabatic wall temperature, T_2 is the secondary air temperature, and T_∞ is the mainstream temperature. During the experiment, the temperature difference $T_2 - T_\infty$ was maintained about 20K. It was actually difficult to achieve an adiabatic wall condition in this test model. Some correction had to be accordingly made on the results of Eq. (4), although a rigorous correction was almost impossible. The method used by Mick and Mayle (1988) was adopted in this study, which yielded the following modification of Eq. (4).

$$\eta = \frac{T_{aw} - T_\infty}{T_2 - T_\infty} = \frac{T_m - T_\infty - \Delta T}{T_2 - T_\infty} + \frac{q_{rad} + q_{cond}}{h(T_2 - T_\infty)} , \qquad (5)$$

where T_m is the measured surface temperature, ΔT is the surface temperature correction, h is the heat transfer coefficient influenced by the injected air, q_{rad} and q_{cond} are the radiative and conduction heat flux from the surface, respectively. ΔT consists of two parts; one is the effect of back surface heating and the other is the effect of ill-positioning of the hot junctions of the thermocouples under the test surface. The magnitude of the latter effect was determined by the preliminary test. The former effect seems to depend on the temperature difference between the front and back side of the test model $(T_2 - T_w)$. In this study, on a basis of the finding by Mick and Mayle, it was assumed that the magnitude of ΔT was about 5% of $(T_2 - T_w)$. For simplicity, we also assume that q_{rad} and q_{cond} cancel each other.

An uncertainty analysis based on the method of Kline and McClintock (1953) was carried out for the film effectiveness. The uncertainty of film effectiveness, including the effects of the above-mentioned assumptions, was about 6% over the leading edge region except for the rim regions of the cooling holes and less than 12% for the far downstream of the holes.

RESULTS AND DISCUSSION

Velocity Distribution

Figure 5 shows the experimental results of the velocity distribution as well as the heat transfer distribution ($Nu_D/Re_D^{0.5}$) around the leading edge of the test model, accompanied by the corresponding potential flow analysis by use of BEM (Boundary Element Method). These data

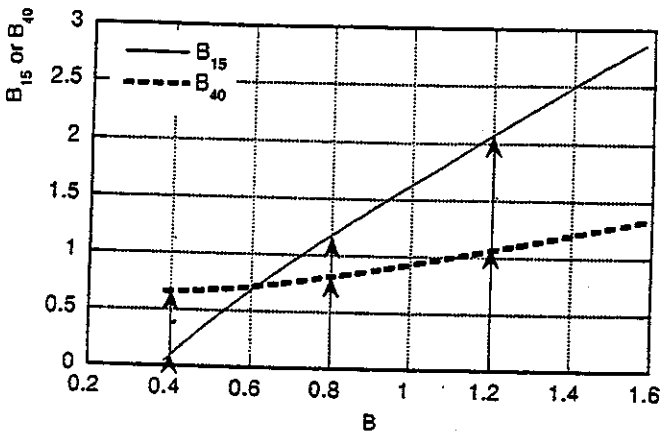

Figure 4 Relationship of local and mean blowing ratio

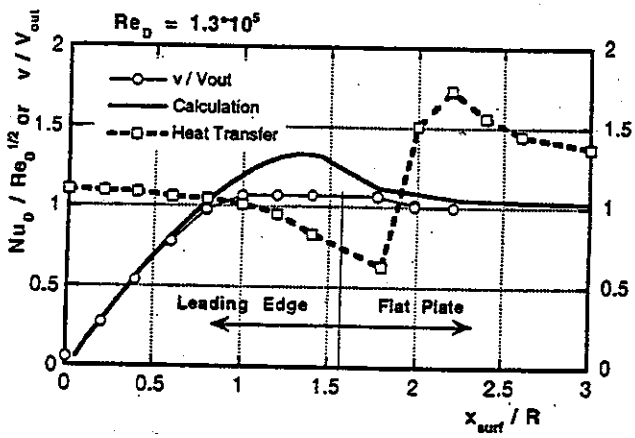

Figure 5 Velocity and heat transfer distributions

show that there was a separation bubble around the junction of leading edge and flat plate. The separation began at $x_{surf}/R \cong 1$ and reattached at $x_{surf}/R \cong 2$.

It should be noted that these data were for the test model with no cooling holes. In fact, cooling holes or injected air have some influence on the boundary layer over the leading edge, which seems to affect the separation to some extent. To the author's best knowledge, however, few information is available on this point. Therefore the data in Figure 5 can be used as an indicator of a separation bubble. Besides, detailed measurements on the behavior of separation bubble under several disturbances are under way to obtain some insight into this phenomena (Koyabu (1995)).

Free-Stream Turbulence and Wake Turbulence

Characteristics of the free-stream turbulence as well as the wake turbulence obtained in this test facility were already determined by Funazaki et al. (1995), and a summary of those results are documented in the following.

Free-stream turbulence intensity Tu_b decreases along with the distance measured from the turbulence grid. It was found that this could be described by the following expression for each type of the turbulence grids in this study.

$$Tu_b = 10.64\left((L-|x|)/M\right)^{-0.559}, \quad M/d_g \cong 6 \qquad (6)$$

where L is the distance between the turbulence grid and the test model. Eq. (6) was modified in order to account for the blockage effect of the test model upon the turbulence intensity, which resulted in the following expression;

$$Tu_b(x) = 10.64\left((L-|x|)/M\right)^{-0.559} \Big/ \left(1-\left(R/(x-R)\right)^2\right). \qquad (7)$$

Conventionally a reference free-stream turbulence intensity is defined as the minimum value calculated from Eq. (7).

Wake turbulence was measured likewise in the free-stream turbulence case and the data was arranged in terms of peak turbulence intensity within the wake as follows;

$$Tu_{max} = 73.58\left((l-|x|)/d\right)^{-0.67}. \qquad (8)$$

where l is the distance between the bar moving plane and test model. It is recently found that Eq. (9) yields almost the same results as the experimental data given by Halstead et al. (1995).

As for length scale of the free-stream turbulence, a streamwise turbulence dissipation scale L_e, defined as (Hancock and Bradshaw (1983)),

$$L_e = -\left(\overline{u'^2}\right)^{3/2} \Big/ \left(U\, d\overline{u'^2}/dx\right). \qquad (9)$$

can be calculated by use of Eq. (7).

In the nominal setting of the test model L is 300 mm and l is 200 mm and a reference free-stream turbulence and its dissipation length are accordingly determined as documented in Table 1.

Views of Temperature Distributions by Liquid Crystal

Figure 6 shows the front and side views of temperature distributions captured by the liquid crystal under no artificial flow disturbances for $B = 0.4$, 0.8 and 1.2, respectively. Note that white color regions appear in the side views due to the excessive lighting from the above. For the lowest blowing ratio, as indicated in Figure 4, very small amount of the secondary air is injected from the cooling hole in the first row. Moreover, the injected air from the second row is convected almost horizontally along the model surface, covering a limited area on the entire model surface. For $B = 0.8$, injected air from the upper half of the cooling hole in the first row can be identified, which moves and spreads so as to cover the area between the neighboring cooling holes in the second row. Eventually the injected air together with that from the second row covers almost the entire surface after the second row so that the liquid crystal sheet becomes almost green. This suggests that the blowing ratio $B = 0.8$ will yield high values of spanwise averaged film effectiveness. For the highest blowing ratio $B = 1.2$, because of its high spanwise momentum flux, the injected air is gradually drifted in the spanwise direction along the model surface. One might notice that mergers happen between the injected airs from the first and the second rows, which ends up with the appearance of uncovered regions by the injected air.

Local Film Effectiveness Distribution

General features. Figure 7 shows local film effectiveness distributions on the unfolded surface of the test model for three blowing ratios in the "no wake (S = 0)" condition with low free-stream turbulence (No Grid). Figure 7 also contains rough sketches of Figure 6 indicating

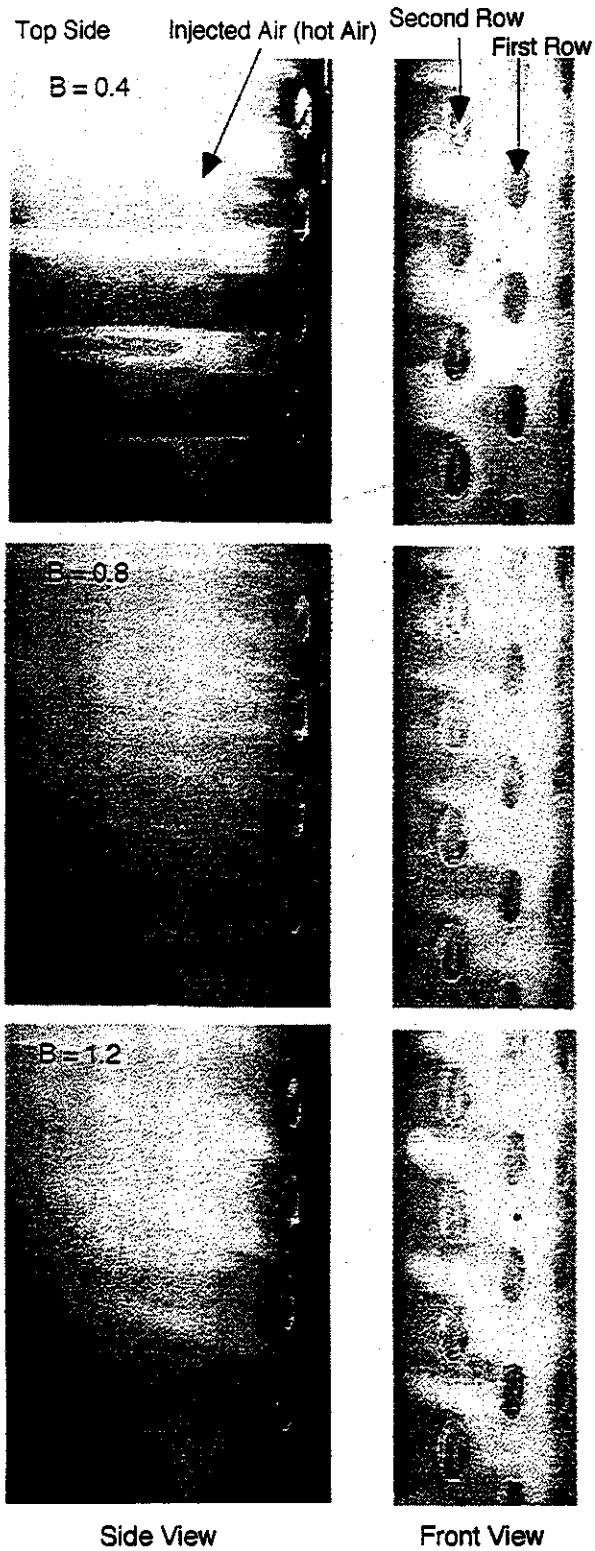

Figure 6 Views of temperature distributions near the cooling holes obtained by the liquid crystal (No Grid / S = 0)

the coverage of the injected airs from the cooling holes. Note that the bottom line of the unfolded surface in Figure 7 corresponds to the top line of Figure 3. Therefore, y coordinate in Figure 7 is directed toward the bottom of the test model.

Figure 7 reveals a clear relationship between the injected air and film effectiveness appearing at each measuring location. For $B = 0.4$, since only a small amount of secondary air comes from the cooling holes in the first row, the film effectiveness downstream of the first row is low. On the other hand, the film effectiveness downstream of the second row, especially at the upper side of the cooling hole, becomes considerably high, which results in large spanwise variation of the film effectiveness. For $B = 0.8$, the injected air covers almost the entire surface of the test model, so that we obtain relatively high values of film effectiveness over the surface. For $B = 1.2$, the injected air drifts towards the top side of the test model and eventually there appear regions behind the second row that are not covered by the injected air. This results in significant spanwise variation in film effectiveness downstream of the second row. Observations from the side view angle also show that the injected air tends to spread on the surface and those uncovered regions gradually disappear towards the aft portion of the test model.

Salcudean et al. (1994) have recently obtained contours of iso-film effectiveness near the cooling holes similar to those of the present study. However, dependencies of those results on the blowing ratio B slightly differs with each other, probably because of the difference in the location of the second row, e.g., ±40° for the present case, whereas ±44° for the case of Salcudean et al.

Effect of the wake passing. Figure 8 shows deviations of the film effectiveness of the cases of $S = 0.40$ measured from the cases of $S = 0.0$ (No Wake) for three blowing ratios under low free-stream turbulence. Note that the positive value stands for increase in film effectiveness from the corresponding base data (No Grid, $S = 0.0$), whereas the negative value stands for the decrease. For the blowing ratio $B = 0.4$, the wake-affected film effectiveness shows overall decrease, with some spots of slight increase. For the blowing ratio $B = 0.8$, which yields almost full coverage of the injected air over the model surface as shown in the above, significant decreases in film effectiveness occurs behind the second row. One might notice that the effect of the wake passing does not appear in a symmetric manner with respect to the stagnation line $x_{surf} / R = 0$. One of possible explanations on this phenomenon is the effect of wake slip velocity (Kerrebrock and Mikolajczak (1970) or a so-called negative jet of the wake. The other plausible explanation could be a contribution of wake-induced variation in local mass flux from each of the cooling holes to the film effectiveness. However no information is available to verify these suppositions yet. For $B = 1.2$, meaningful and somewhat surprising increases in film effectiveness are observed after the second row. Actually Mehendale and Han (1992) reported similar findings in their study even under the influence of intense turbulence with about 10 %. The authors think for $B = 1.2$ the wake passage effectively promote the spanwise mixing of the secondary air jets from the first and second rows that are overlapped with each other, so as to increase the area of film coverage.

Effect of free-stream turbulence. Figure 9 shows deviations of the film effectiveness of the cases of Grid 3 measured from the cases of No Grid for three blowing ratios with no influence of the wake. For the blowing ratio $B = 0.4$, the film effectiveness surprisingly increases over almost the whole area of the measured test surface. Even for higher blowing ratio cases a considerable number of spots with meaningful increase in film effectiveness appear, however, the effect of the enhanced-free-stream turbulence tends to weaken with the blowing ration. Likewise in the above, this increase can be attributed to the effect of the enhanced spanwise mixing by the free-stream turbulence,

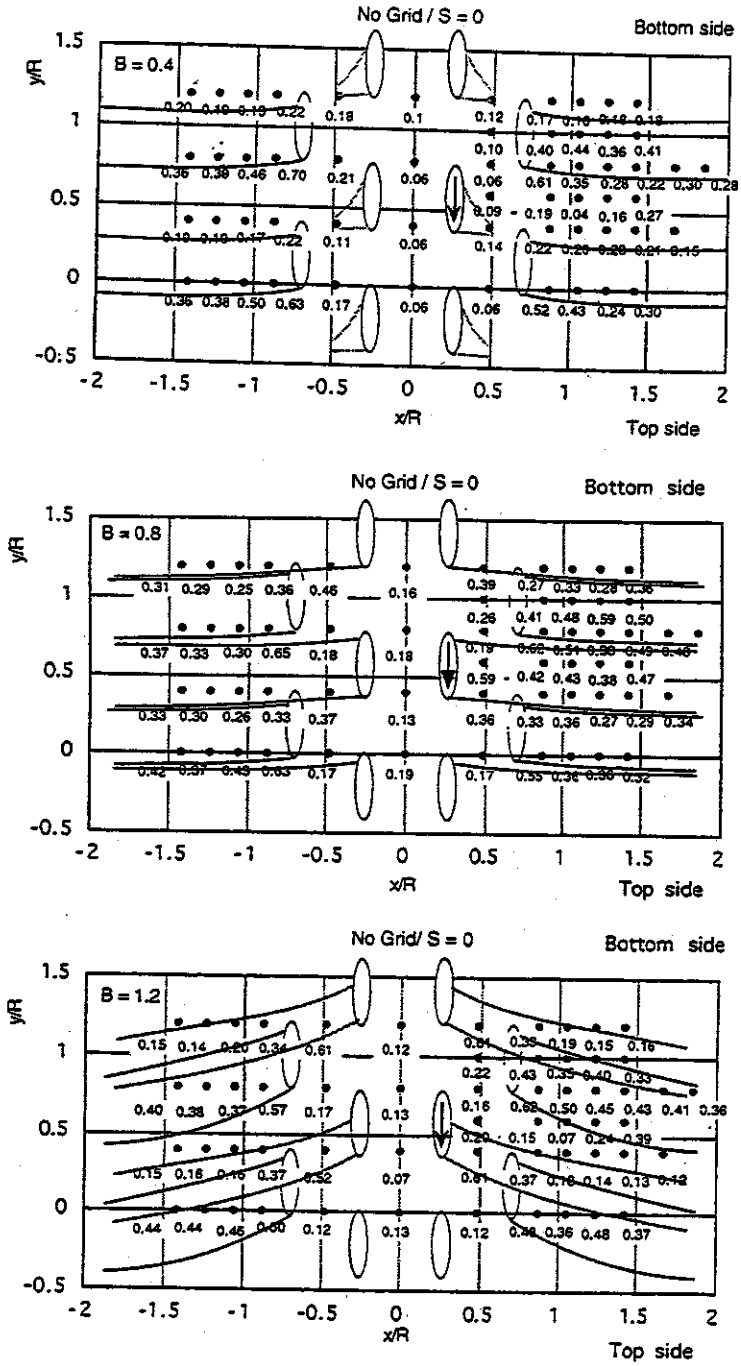

Figure 7 Local film effectiveness distributions near the holes with sketches of the coverage of the injected air (No Grid / S = 0)

similar to the findings by Mehendale and Han (1992), where the ratio of hole pitch to hole diameter was 3.

Spanwise mixing enhanced by the free-stream turbulence or by the wake passage is seemingly a plausible explanation to the local increase in film effectiveness, however, the authors feel great necessity to verify whether it is truly the case. Therefore temperature measurement of the flow field near the cooling holes is now under way.

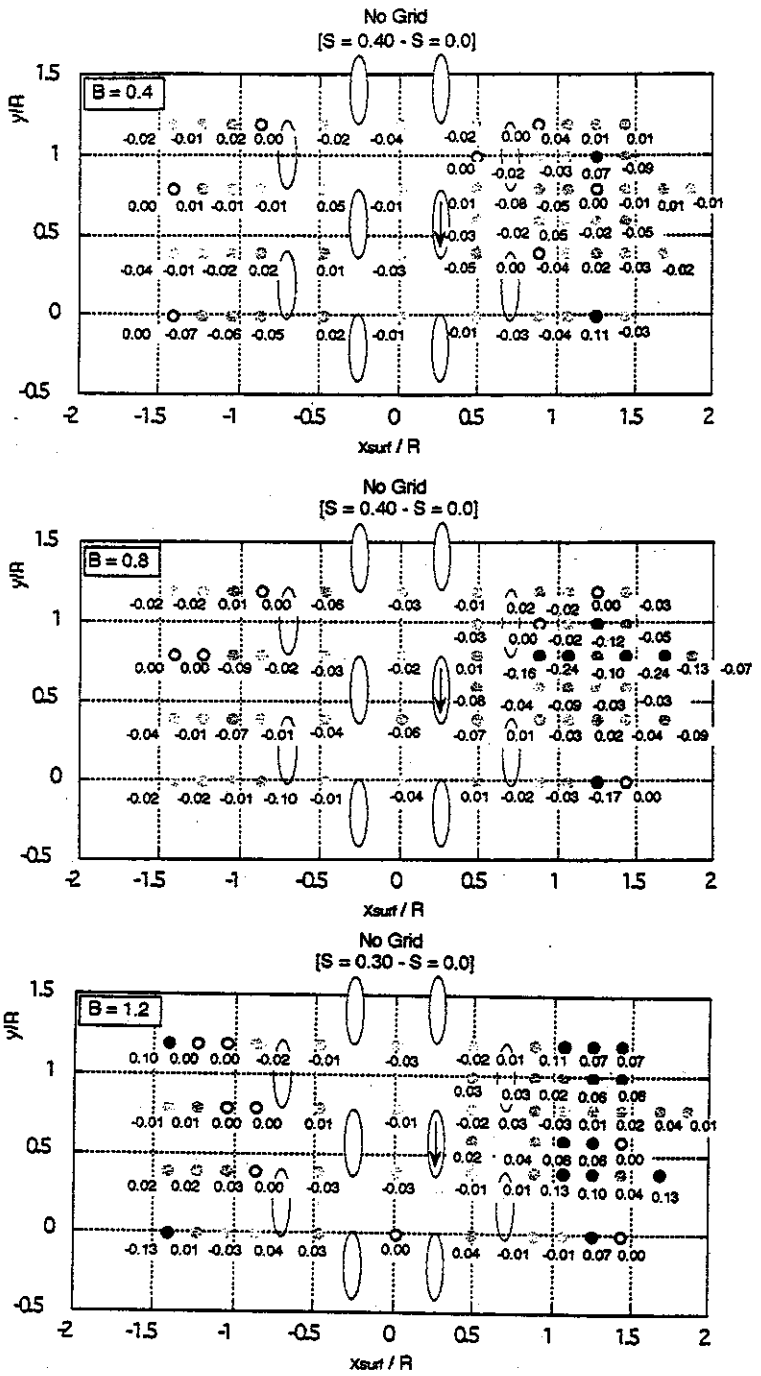

$-0.05 \le \Delta\eta < 0$ $0 < \Delta\eta \le 0.05$

$-0.1 \le \Delta\eta < -0.05$ $0.05 < \Delta\eta \le 0.1$

$\Delta\eta < -0.1$ $0.1 < \Delta\eta$

Figure 8 Differences in film effectiveness between S = 0.4 and S = 0 with low free-stream turbulence

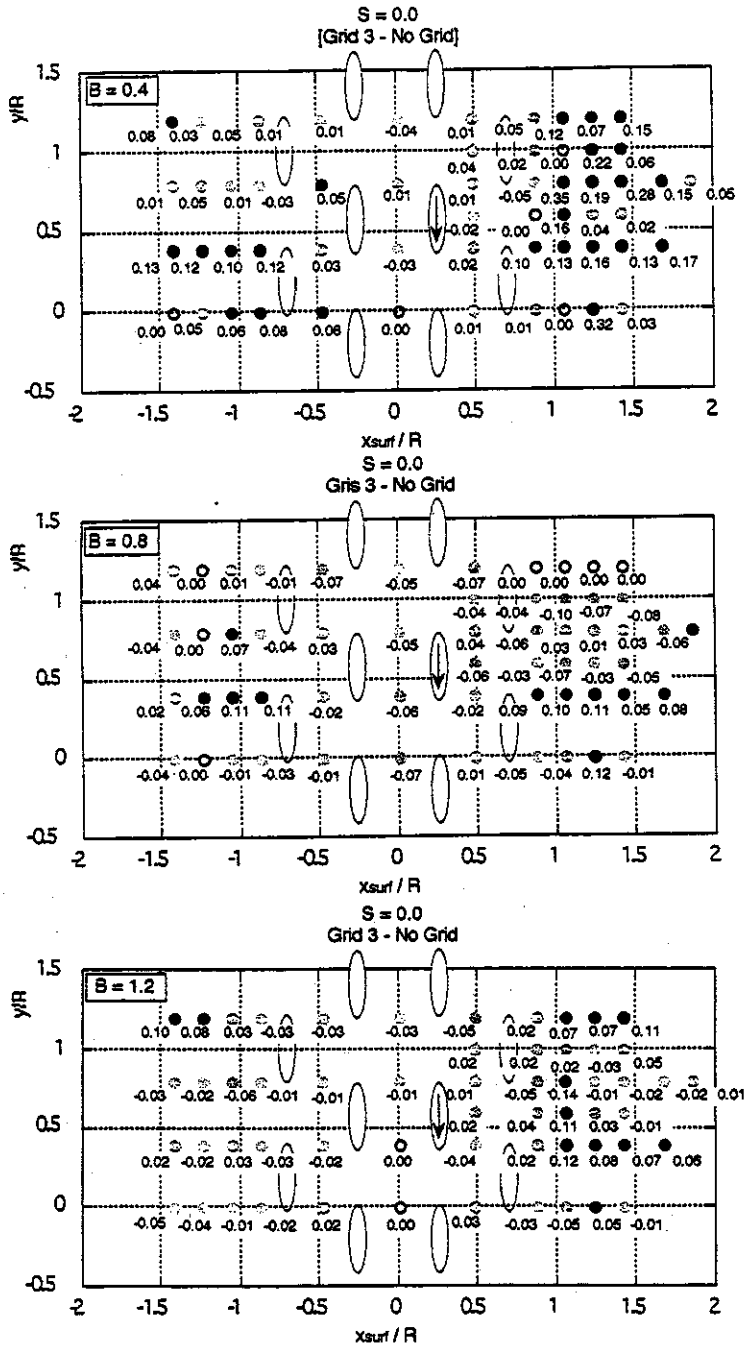

Figure 9 Differences in film effectiveness between Grid 3 and No Grid with no wake effect

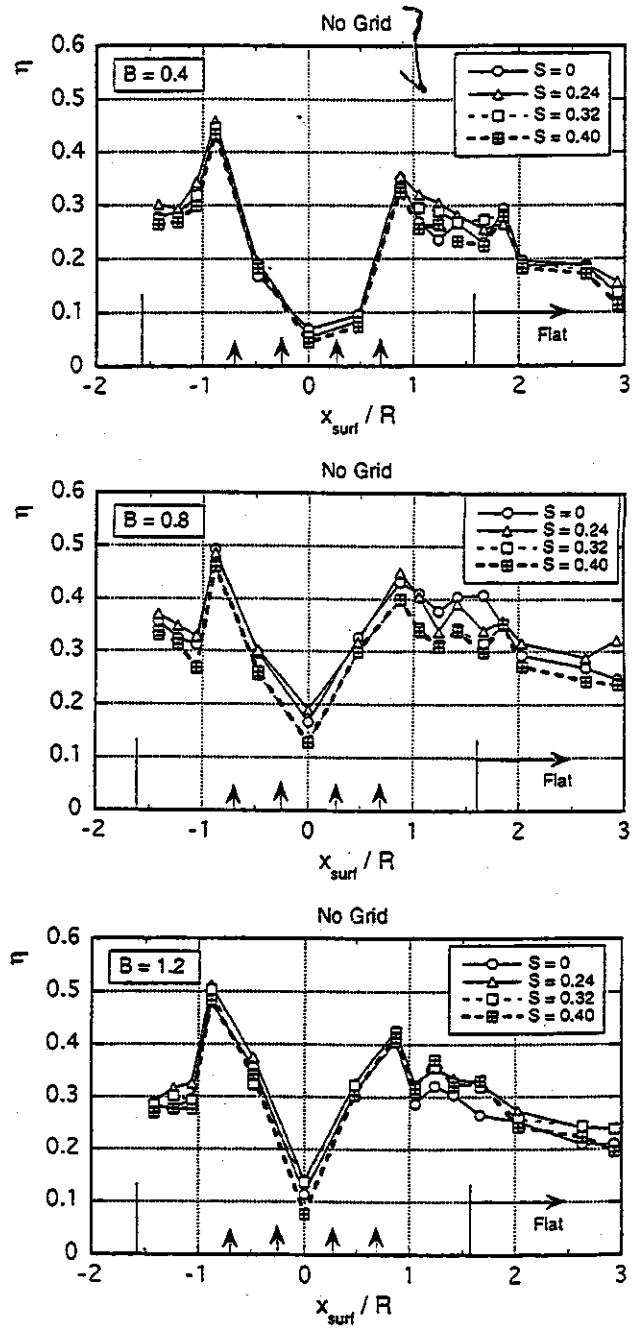

Figure 10 Effect of wake passage upon the spanwise averaged film effectiveness for three blowing ratios (No Grid)

Spanwise-Averaged Film Effectiveness

General features. Figure 10 shows the plots of spanwise averaged film effectiveness for three blowing ratios under the influence of the wake passing. As seen in the local film effectiveness, spanwise-averaged film effectiveness are not symmetric with respect to the stagnation line, $x_{surf}/R = 0$, especially for $B = 0.4$. In addition to the fact that sample numbers for averaging are different between both sides as shown in Figure 3, it seems that mass flow rates from the holes at +15° and −15° are difference, especially in this lowest blowing ratio, which contributes to this asymmetry. Hereafter the discussion is focused on the data on the right-hand side ($x_{surf}/R \geq 0$) of these plots.

Generally the maximum appears after the second row of the film holes, followed by gradual decrease due to the dilution of the injected air. For $B = 0.8$, this decreasing rate is relatively slow compared to

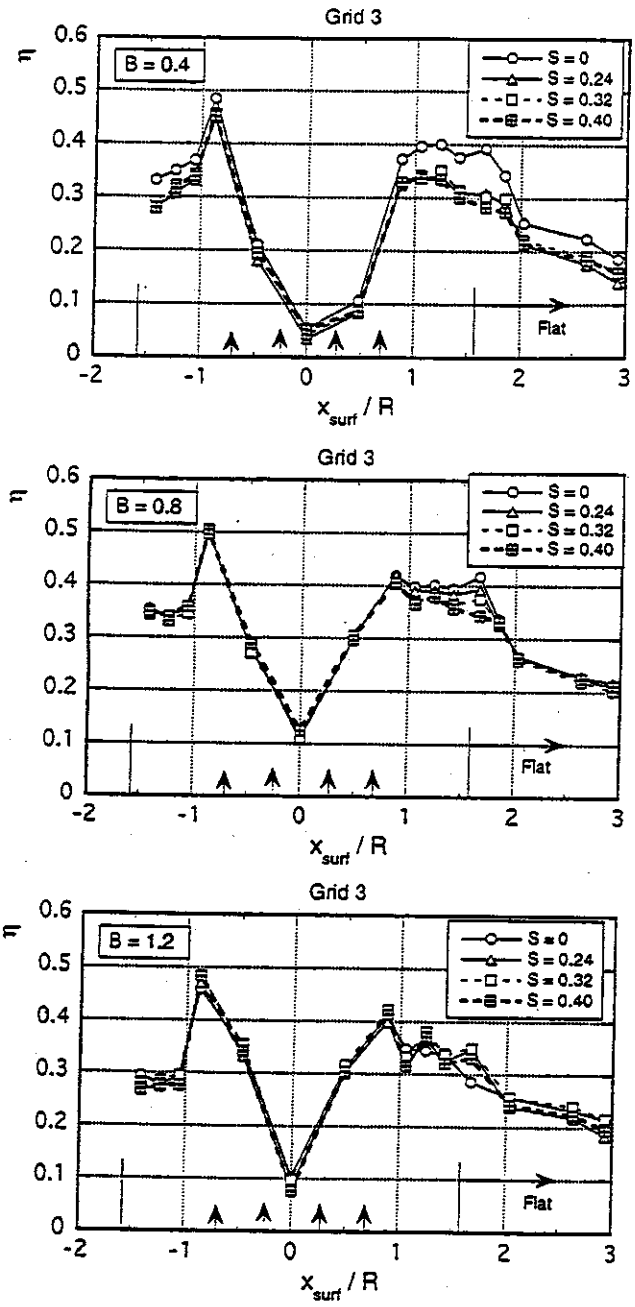

Figure 11 Effect of wake passage upon the spanwise averaged film effectiveness for three blowing ratios (Grid 3)

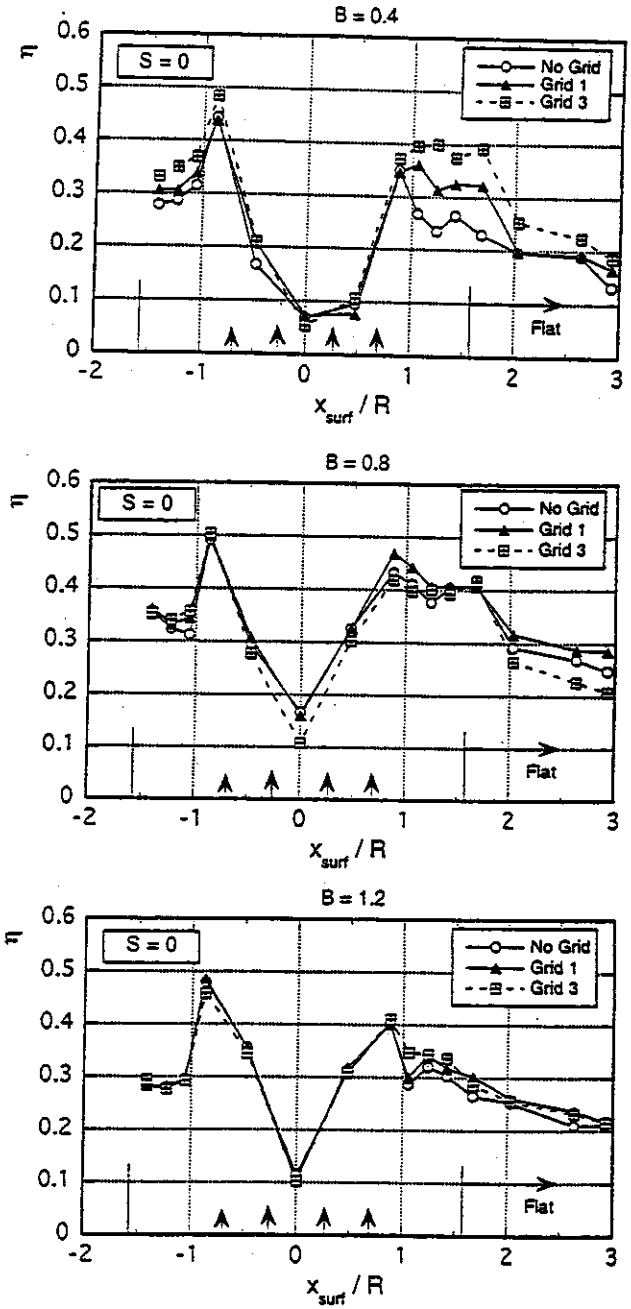

Figure 12 Effect of enhanced free-stream turbulence on the spanwise averaged film effectiveness for three blowing ratios (S = 0)

other cases, which results in the highest spanwise-averaged film effectiveness over the model surface among three blowing ratio cases, as can be expected from the local film effectiveness distributions. In the case of $B = 1.2$, there appears a small valley of the film effectiveness after the maximum, probably due to the spanwise variation of the local film effectiveness as identified in the above.

Effect of the wake passage. As the Strouhal number increases, the averaged film effectiveness tends to decrease for $B = 0.4$ and $B = 0.8$. However, for $B = 1.2$, the averaged film effectiveness rather exhibits a slight increase, as seen in the local film effectiveness distribution.

Figure 11 shows spanwise averaged film effectiveness under the influence of the wake passing as well as enhanced free-stream turbulence from Grid 3. Except for the case of $B = 0.4$ and the data obtained around the separation zone for $B = 0.8$, no discernible effect of the wake passage upon the average film effectiveness can be found. As for

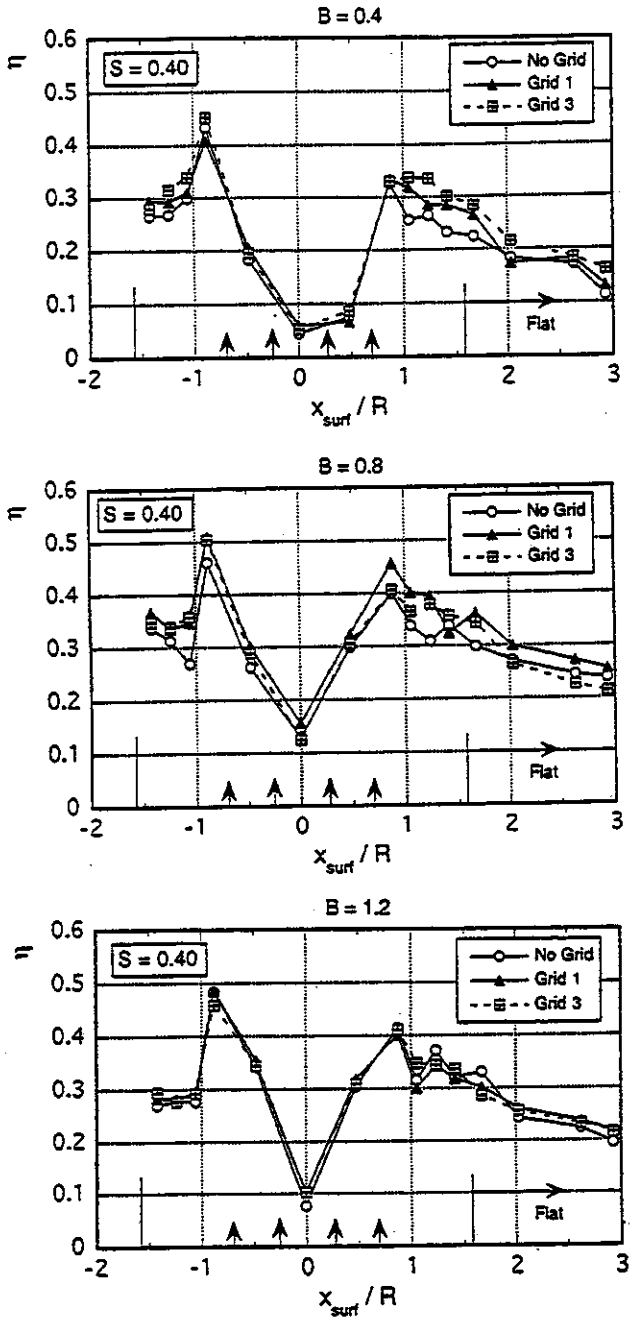

Figure 13 Effect of enhanced free-stream turbulence on the spanwise averaged film effectiveness for three blowing ratios (S = 0.40)

the case of $B = 0.4$, the reason for the notable decrease in the averaged film effectiveness with the increase of Strouhal number is not certain. However, it can be concluded that the wake passage over the test model reduces the film effectiveness in the case of low and moderate blowing ratios.

Effect of free-stream turbulence. Figures 12 and 13 show the effect of free-stream turbulence on the spanwise-averaged film effectiveness for three blowing ratios without and with the influence of the periodic wakes. It follows from these data that, regardless of the influence of the wake passage, free-stream turbulence does not have any significant impact on the spanwise-averaged film effectiveness for $B = 1.2$. For the case of $B = 0.4$, augmented free-stream turbulence surprisingly increases the averaged film effectiveness over the region ranging from $x_{surf}/R = 1 - 2$. Note that this region almost corresponds to the area where the separation occurs. This tendency does not change under the influence of the wake passing, although the effect of the free-stream turbulence becomes small though (see Figure 13). For a moderate blowing ratio $B = 0.8$, the enhanced free-stream turbulence appears to decrease the average film effectiveness to some extent, however, its effect almost diminishes under the influence of the wake passage.

CONCLUSIONS

Detailed studies were conducted on film effectiveness of inclined discrete film holes around the leading edge of a blunt test model of a turbine blade that was subjected to periodically incoming wakes as well as free-stream turbulence with various levels of intensity. Important findings, useful for designing film-cooled turbine blades, were obtained in the studies. Summary of this paper is itemized as follows;

1. Observations by use of the liquid crystal revealed the extent of film coverage near the film holes at the leading edge. At the lowest blowing ratio $B = 0.4$, the secondary air from the film holes in the first row could not be identified and the air from the holes in the second row was convected almost horizontally. At the blowing ratio $B = 0.8$, the injected air from the holes in the first and the second rows tended to cover almost the entire surface of the test model behind the second row. Further increase in blowing ratio caused spanwise drift of the injected air, which led to an appearance of uncovered region by the injected air.
2. From the local film effectiveness distributions, accompanied by the sketches of the injected air trajectories, it was found the blowing ratio $B = 0.8$ produced relatively small spanwise variation in film effectiveness compared to the other blowing ratio cases. This was because the injected secondary air achieved almost full coverage.
3. Generally, distributions of the spanwise averaged film effectiveness exhibited the maximum just behind the second row, followed by gradual decrease towards the downstream. On the average, the blowing ratio $B = 0.8$ yielded relatively high film effectiveness. Periodic wake passage usually deteriorated the spanwise film effectiveness. On the other hand, enhanced free-stream turbulence did not always deteriorated the film effectiveness drastically, sometimes it caused a slight increase in the film effectiveness. The effect of the free-stream turbulence tended to diminish with the increase in Strouhal number.

ACKNOWLEDGMENTS

The authors are greatly indebted to Mr. M. Yokota, former graduate student of Iwate University, for his contribution to the present study.

REFERENCES

Funazaki, K., 1994, "Studies on Wake-Affected Heat Transfer around the Circular Leading Edge of Blunt Body," ASME Paper 94-GT-25.

Funazaki, K., Yamawaki, S. and Maya, T., 1995#1, "Studies on Wake-Affected Heat Transfer around the Leading Edge of a Blunt Body," Proceedings of the 3rd ASME/JSME Thermal Engineering Conference, Vol. 1, pp. 343 - 350

Funazaki, K., Yokota, M. and Yamawaki, S., 1995#2, "The Effect of Periodic Wake Passing on Film Effectiveness of Discrete Cooling Holes around the Leading Edge of a Blunt Body," ASME Paper 95-GT-183.

Halstead, D. E., Wisler, D. C., Okiishi, T. H., Walker, G. J., Hodson,

H. P. and Shin, H. W., 1995, "Boundary Layer Development in Axial Compressor and Turbines, Part 4 of 4: Computations and Analysis," ASME Paper 95-GT-464.

Hancock, P. E. and Bradshaw, P., 1983, "The Effect of Free-Stream Turbulence on Turbulent Boundary Layers," ASME Journal of Fluids Engineering, Vol. 105, pp. 284-289.

Kerrebrock, J. L. and Mikolajczak, A. A., 1970, "Inter-Stator Transport of Rotor Wakes and Its Effect on Compressor Performance," Trans. ASME Journal of Engineering for Power, Vol. pp. 359 - 370.

Kline, S. J. and McClintock, F. A., 1953, "Describing Uncertainties in Single Sample Experiments," Mechanical Engineering, Vol. pp. 3-8.

Koyabu, E., 1995, "Studies on the Behavior of a Separation Bubble on a Blunt Body under the Influence of the Wake Passage," Bachelor thesis, Iwate University

Mehendale, A. B. and Han, J. C., 1992, "Influence of High Mainstream Turbulence on Leading Edge Film Cooling Heat Transfer," ASME Journal of Turbomachinery, Vol. 114, pp. 707 - 715.

Mick, W. J. and Mayle, R. E., 1988, "Stagnation Film Cooling and Heat Transfer, Including Its Effect Within the Hole Pattern," ASME Journal of Turbomachinery, Vol. 110, pp. 66-72.

Salcudean, M., Gartshore, I., Zhang, K. and McLean, I., 1994, "An Experimental Study of Film Cooling Effectiveness Near the Leading Edge of a Turbine Blade," Trans. ASME Journal of Turbomachinery, Vol. 116, pp. 71 - 79.